Int. J. Adv. Appl. Math. and Mech. 3(3) (2016) 1 – 15 (ISSN: 2347-2529)

Journal homepage: www.ijaamm.com

IJAAMM

International Journal of Advances in Applied Mathematics and Mechanics

Analytical solution of fully developed gaseous slip flow in elliptic microchannel

Research Article

Samir K. Das[a, *], **Farzad Tahmouresi**[b, c]

[a] *Department of Applied Mathematics, Defence Institute of Advanced Technology, Deemed University, Girinagar, Pune-411025, India*

[b] *Department of Mathematics, College of Science, Kermanshah Branch, Islamic Azad University, Kermanshah-6718997551, Iran*

[c] *Department of Mathematics, Savitribai Phule Pune University, Pune-411007, India*

Received 06 August 2015; accepted (in revised version) 05 November 2015

Abstract: The paper presents an analytical solution of velocity for fully developed gaseous slip flow in elliptic microchannels. We investigate fully developed laminar hydrodynamically steady state and incompressible slip flow with constant fluid properties. The governing equation are solved analytically for various aspect ratios using elliptic cylindrical coordinate system on applying integral transform technique to analyze gaseous slip flow in micro-channels. Prior to apply integral transform technique, Arfken transform was used on momentum equations and first-order slip boundary conditions at each channel walls were imposed. Based on the selection of a characteristic length scale, the square root of cross-sectional area, the effect of duct shape has been minimized. The results of a normalized Poiseuille number (Po) for elliptic micro-channels show very good improvement with the previous results of rectangular and elliptic micro-channels. Further, it is also observed that the present values of friction factor and Reynolds number product (fRe) shows good agreement for smaller aspect ratios (ε).

MSC: 35A22 • 76R10

Keywords: Slip flow • Elliptic microchannels • Normalized Poiseuille number • Arfken transform • Integral transform technique

1. Introduction

In the past years, studies on micro-channel flow passages have become necessary due to the rapid development of micro-fluidic devices used for several engineering applications such as micro electro-mechanical systems (MEMS), integrated cooling of microelectronic circuits, digital microprocessors, micro-reactors, high-frequency fluidic control systems, fuel cell technology, medical devices, high heat-flux compact heat exchangers and so on.This has created intensive interest among the researchers to investigate various aspects of microscale transport phenomena and fundamental aspects of micro-fluidic devices to understand the flow characteristics in micro-channels, pressure distribution and heat transfer properties. The major advances of industrial technologies in the past are the MEMS device which is having a characteristic length of less than 1 mm whereas greater than 1 μm non-continuum behavior is significant. Although several experimental and investigations are available for the number of principal problems, the problems related to micro-fluid hydrodynamics are not well understood. However, there is contradiction related to drag in micro-channels and transition from laminar to turbulent flow which leads to difficulty in understanding the phenomenon. The investigations on gas flow in micro-channels has emerged as an important area of research due to its applications in gas chromatography, micro-chemical gas reactors, gas flow sensors, low-pressure semiconductor manufacturing machines, microscale heat exchangers and micro gas regulators. In recent years, micro-channels with different cross-sectional geometries were fabricated for both commercial and scientific purposes.

* Corresponding author. Tel.: +91 20 24304081; Fax: +91 20 24389288.
E-mail addresses: samirkdas@diat.ac.in, samirkumar_d@yahoo.com (Samir K. Das), tahmouresif@iauksh.ac.ir, tahmouresif@yahoo.com (Farzad Tahmouresi)

Nomenclature

A_c	Area of ellipse (m^2)
A_n, I_1, I_2, I_3	Variables defined for simplicity
a	Major semi-axis of ellipses (m)
b	Minor semi-axis of ellipses (m)
c	Half focal length of ellipses (m)
D_h	Hydraulic diameter = $4A_c/P_c$
e	eccentricity = $\sqrt{1-b^2/a^2}$
$E(e)$	Complete elliptical integral of the second kind
f	Fanning friction factor
f Re	Friction factor and Reynolds number product
h_ξ, h_η, h_z	Scale factors for the elliptic cylindrical coordinate (m)
K_n	Knudsen number = λ/L_c
L_c	Characteristic length scale(m)
N	Normalization integral
n	Normal direction to the wall
p	Pressure (N/m^2)
P_c	Perimeter of ellipses (m)
P	Normalized pressure gradient
Po	Poiseuille number = $\tau D_h/\mu u_m$
Re	Reynolds number = $D_h u_m/\upsilon$
u	Gaseous velocity component in z direction (m/s)
u_m	Mean velocity (m/s)
u_s	Slip velocity (m/s)
u_ξ	Filtering function in the ξ-direction
x, y	Cartesian coordinates (m)
z	Coordinate in flow direction (m)

Greek symbols

β_υ	Nondimensional variable defined by Eq. (3)
β	Dimensionless slip parameter $(=\beta_\upsilon Kn)$
β_s	Slip coefficient
Γ	Inside periphery of microchannel (m)
μ	Eigenvalue
ε	Aspect ratio = b/a
λ	Molecular mean free path (m)
μ	Dynamic viscosity (Ns/m^2)
ξ, η	Nondimensional elliptic cylinder coordinates
ξ_0	Parameter of elliptic cylinder coordinates
σ_υ	Tangential momentum coefficient
τ	Wall shear stress (N/m^2)
υ	Kinematic viscosity (m^2/s)
Ω	Cross-section of microchannel
ψ	Eigenfunction

Subscripts

ns	No-slip

The Knudsen number (Kn) can be defined as the ratio of the molecular mean free path (λ) of gas to the characteristic length scale (L_c) of the channel or duct which is widely used to classify the continuum flows and for small values of Knudsen number ($Kn = \lambda/L_c \leq 10^{-3}$). For large Knudsen number ($Kn = \lambda/L_c \geq 10$), the fluid flow can be considered as free molecular flow and in the intermediate range of Knudsen number ($10^{-3} \leq Kn = \lambda/L_c \leq 0.2$), slip flow regime starts which can be modeled based on Navier-Stokes equations with slip conditions at the walls. Usually the characteristic length scale of the gas flow in a micro-channel varies from 1 to 100 μm and the mean free path of

most common gases is approximately 60 nm at atmospheric conditions Karniadakis et al.[1]. In usual applications, characteristic lengths are in the range of approximately 10 to 200 μm and therefore gas flows in the micro-channels are often considered in the slip flow regime Gad-el-Hak [2] and Jang et al.[3].

The elliptic cross-section is one such useful channel shape that may be produced by microfabrications for which vary few literatures is available. In this paper, fully developed gaseous slip flow behavior in elliptic micro-channels investigated analytically. First-order slip boundary conditions are considered at each channel walls and normalized Poiseuille number is obtained and compared with the existing analytical and numerical solutions for variety of geometries. The effects of channel aspect ratio and Knudsen number (Kn) is discussed with respect to normalized Poiseuille number.

2. Literature review

During last two decades flow and heat transfer in micro-channel and nano-channels have received considerable attention due its significant applications in micro-elctronic devices. The development of microscale fluid systems has also motivated great interest in this field of study. Arkilic et al. [4], Liu et al. [5], Pfahler et al. [6, 7], Harley et al. [8], Wu et al. [9] and Araki et al. [10] investigated experimentally micro-fluidic devices for small length scales to understand rarefaction effects. The slip-flow model for a rectangular channel to analyze the effect of slip condition on velocity distribution, compressibility and pressure drop using analytical method was developed by Ebert and Sparrow [11]. With respect to continuum flow, the effects of slip reduce velocity distribution whereas the effect of compressibility increases the pressure drop through an increase in the viscous shear. Usually, slip-flow regimes are modeled based on Navier-Stokes and energy equations by considering boundary conditions in order to include rarefaction effects on the velocity and temperature fields. From the monographs of Eckert and Drake [12], the detailed study can be obtained. Arkilic et al.[4] investigated gaseous flow analytically and experimentally by using two-dimensional Navier-Stokes equations to demonstrate the effects of compressibility and rarefaction using the long micro-channel and rarefaction effect. Liu et al. [5] obtained solution of Navier-Stokes equation using slip flow boundary conditions which shows good agreement with the experimental data for micro-channel flows. For small length scales rarefaction effects are important which is evident from the experiments conducted by Pfahler et al. [6, 7], Harley et al. [8], Wu et al.[9] and Araki et al. [10]. This also confirms that continuum analyses are unable to predict the flow properties for transport of gases in micro-size devices. A detailed review of the research so far and analysis for liquid flow and gas flow can be found in the investigations of Rostami et al. [13, 14]. Morini et al. [15] investigated the rarefaction effects on the pressure drop through silicon micro-channels having rectangular, trapezoidal and double-trapezoidal cross sections. For the lower aspect ratios rarefaction effects on the Poiseuille number found to be much stronger and the effect of Knudsen number for friction factor reduction is also discussed. Based on experimental work of Araki et al. [10] on gaseous flow in trapezoidal microchannels show that friction factor is lower than that predicted by conventional theory, this helps to understand the deviation was caused by the rarefaction effects. Aubert and Colin [16] investigated slip-flow model based on second-order boundary conditions for gaseous flow in rectangular micro-channels as proposed by Deisler [17]. Colin et al. [18] developed experimental setup for the measurement of gaseous microflow rates under controlled temperature and pressure conditions. Although, number of researchers has attempted to develop second-order slip models to account second order slip coefficient that can be used for transition regime, nevertheless a universally accepted second-order slip coefficient model does not exist Barron et al. [19]. Duan and Muzychka [20, 21] developed an analytical slip-flow solution for non-circular and elliptic microchannels to predict friction factor and Reynolds number product fRe and the Poiseuille number. The accuracy of the developed model was found to be within 10% and for elliptic microchennels the accuracy lies between 3% of the exact value for the non-circular micro-channels. To predict the friction factor and Reynolds number product fRe for slip flow, Duan and Yovanovich [22] developed a simple model using normalized Poiseuille number. It was observed that for normalized Poiseuille number has an accuracy of 4.2% for all common duct shapes where the range of shape that includes circle, ellipse, rectangle, star-shape, triangle, square and hexagon to predict velocity distribution and pressure drop. Tunc and Bayazitoglu [23] obtained an analytical slip-flow solution to predict slip coefficient, to represent the velocity slip a parameter called “slip coefficient” was defined as the ratio of the velocity of the fluid at the wall to the mean velocity. The variation of this parameter with the Knudsen number has been shown for different aspect ratios. For the same Knudsen number as the aspect ratio becomes smaller, the value of the slip coefficient increases. Tahmouresi and Das [24] investigated the fully developed gaseous slip-flow behavior in symmetric and non-symmetric parabolic micro-channels analytically. Normalized Poiseuille number and pressure distribution are compared with the existing numerical and analytical solutions for different geometries and found good agreement for small aspect ratio with the previous results for rectangular micro-channels. The effects of velocity slip and Joule heating on peristaltic flow of MHD Newtonian fluid in a porous channel with elastic wall properties have been studied under the assumptions of longwavelength and low-Reynolds number by Reddy and Reddy [25]. The analytical solution has been derived for the stream function, temperature and heat transfer coefficient. The emerging flow parameters on the velocity, temperature and heat transfer coefficient are presented graphically and are discussed in detail. Anjali Devi and Kumari [26] investigated the slip flow effects on unsteady hydromagnetic flow over a stretching surface with thermal radiation heat transfer. Resulting non dimensional velocity and temperature profiles are then presented graphically for different values of the parameters involved. Results for skin friction coefficient and the non dimensional rate of heat transfer

are also obtained and are discussed in detail. An numerical analysis has been performed to study the problem of fully developed flow of a fourth grade non- Newtonian fluid between two stationary parallel plates in the presence of an externally applied uniform vertical magnetic field by Ghasemi Moakher et al. [27]. Slip conditions is taken into account at the wall of the channel. The influence of the some physical parameters such as the Slip parameter, non Newtonian parameter and magnetic field parameter on non-dimensional velocity profiles is considered. Also the results reveal that the CM can be used for solving nonlinear differential equations with Robin mixed condition easily.

In the present paper, we develop analytical solution of velocity for fully developed gaseous slip flow in elliptic microchannels. By adopting Arfken transform [28] technique and assuming the flow to be steady, laminar and incompressible with constant fluid properties. The first-order slip boundary conditions are considered at each channel wall to predict normalized Poiseuille number. The paper is organized as follows. We first develop mathematical formulation. Subsequently, analytical solution of slip flow model is developed, followed by results and discussion and conclusion.

3. Mathematical formulation

We considered fully developed gaseous slip flow in a straight elliptic microchannel having uniform cross section as shown in Fig. 1(a). where the flow is hydrodynamically steady state, laminar and incompressible with constant fluid

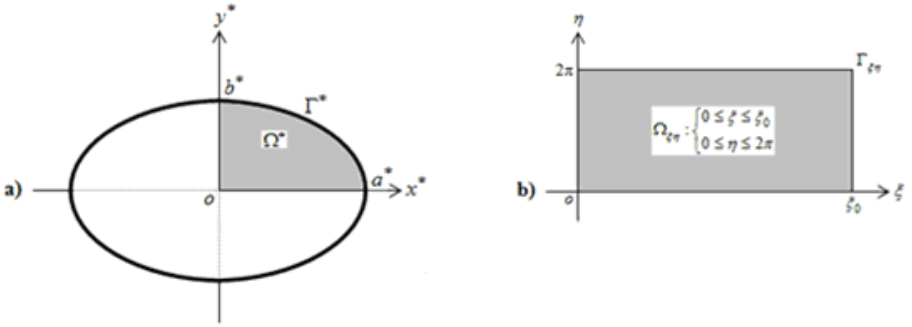

Fig. 1. (a) An elliptic microchannel (b) Non-dimensional transferred microchannel

properties. Assuming the body force terms are neglected, momentum equation with axial velocity in z direction can be expressed as

$$\frac{\partial^2 u^*}{\partial x^{*2}} + \frac{\partial^2 u^*}{\partial y^{*2}} = \frac{1}{\mu}\frac{dp}{dz} \tag{1}$$

and the boundary conditions can be written as follows by Barron et al. [19] and Maxwell [29] based on the assumption that the slip velocity is constant and the same at each boundary

$$u^* = u_s^* = -\beta_v \lambda \left.\frac{\partial u^*}{\partial n^*}\right|_{\Gamma^*} \tag{2}$$

where

$$\beta_v = \frac{2-\sigma_v}{\sigma_v} \tag{3}$$

where n^* is the normal direction to the wall of dimensional elliptic micro-channels, u_s^* is the slip velocity, λ is the molecular mean free path, σ_v is the tangential momentum accommodation coefficient, the value of which typically lies between 0.87 and 1.0 as reported by Rohsenow and Choi [30]. The most usual conditions for σ_v are assumed to have a value of unity. However, the same procedure is valid even if $\sigma_v \neq 1$, defining a general slip parameter as $\beta = \beta_v Kn$, which has been given the range of slip parameter as $0 < \beta < 0.2$. A similar definition of the slip coefficient is also given by Shih et al. [31]. At the end of this section, the slip coefficient can be expressed in terms of the slip parameter. Γ^* represents inside periphery of the following dimensional elliptic microchannel

$$\Omega^* : \frac{x^{*2}}{a^{*2}} + \frac{y^{*2}}{b^{*2}} = 1 \tag{4}$$

3.1. Non-dimensional parameters

The governing equation and the boundary conditions are non-dimensionalized by using the following parameters

$$x = \frac{x^*}{\sqrt{A_c}} \tag{5}$$

$$y = \frac{y^*}{\sqrt{A_c}} \tag{6}$$

$$u = \frac{u^*}{u_m^*} \tag{7}$$

$$a = \frac{a^*}{\sqrt{A_c}} \tag{8}$$

$$b = \frac{b^*}{\sqrt{A_c}} \tag{9}$$

$$n = \frac{n^*}{\sqrt{A_c}} \tag{10}$$

where A_c is the area of the cross-section of elliptic microchannels. Eq. (1) takes the following non-dimensional form

$$\frac{\partial^2 u}{\partial x^2} + \frac{\partial^2 u}{\partial y^2} = P \tag{11}$$

and

$$u = \beta_s = -\beta_v Kn \left.\frac{\partial u}{\partial n}\right|_\Gamma \tag{12}$$

where

$$P = \frac{\left(\sqrt{A_c}\right)^2}{\mu u_m^*} \frac{dp}{dz} \tag{13}$$

$$\beta_s = \frac{u_s^*}{u_m^*} \tag{14}$$

$$\varepsilon = \frac{b^*}{a^*} = \frac{b}{a} \tag{15}$$

where n is the normal direction to the wall of non-dimensional elliptic microchannels, ε is the aspect ratio, β_s is the slip coefficient, which is the measure of the velocity slip at the boundary, P is the normalized pressure gradient, Γ represents inside periphery of the following non-dimensional elliptic microchannel

$$\Omega : \frac{x^2}{a^2} + \frac{y^2}{b^2} = 1 \tag{16}$$

and Kn is Knudsen number which is defined as

$$Kn = \frac{\lambda}{\sqrt{A_c}} \tag{17}$$

3.2. Transformation process

It is convenient to use elliptic cylindrical coordinates Arfken [28] to facilitate the solution process. The orthogonal system of elliptic coordinates (ξ, η) is used to transform the rectangular cross-section in the transformed system(ξ, η) as shown in Fig. 1(b):

$$\begin{cases} x = c cosh\xi cos\eta \\ y = c sinh\xi sin\eta \qquad 0 \le \xi \le \xi_0 \qquad 0 \le \eta < 2\pi \\ z = z \end{cases} \tag{18}$$

The parameter ξ_0 is related to the major and minor axes through

$$\xi_0 = Arc\tanh(\varepsilon) = \ln \frac{1+\varepsilon}{\sqrt{1-\varepsilon^2}} \tag{19}$$

The half focal length of ellipses c is defined such that

$$c = \frac{a}{cosh\xi_0} = \frac{b}{sinh\xi_0} \tag{20}$$

The coefficients h_ξ, h_η, h_z and Jacobian J of the transformation of the system of coordinates (x, y) into the system (ξ, η) are given by

$$h_\xi(\xi,\eta) = h_\eta(\xi,\eta) = c\sqrt{cosh^2\xi - cos^2\eta} \tag{21}$$

$$h_z(\xi,\eta) = 1 \tag{22}$$

$$J(\xi,\eta) = \frac{\partial(x,y)}{\partial(\xi,\eta)} = c^2\left(cosh^2\xi - cos^2\eta\right) \tag{23}$$

In elliptic cylindrical coordinates, the velocity profile becomes

$$\frac{\partial^2 u}{\partial\xi^2} + \frac{\partial^2 u}{\partial\eta^2} = c^2\left(cosh^2\xi - cos^2\eta\right)P \tag{24}$$

The velocity distribution must satisfy the slip boundary condition at the walls. The local slip velocity is proportional to the local velocity gradient normal to the wall. In elliptic cylinder coordinates, the boundary conditions assuming a one quarter basic cell are

$$\frac{1}{h_\eta(\xi,\eta)}\frac{\partial u}{\partial\eta} = 0 \qquad at \qquad \eta = 0 \tag{25}$$

$$\frac{1}{h_\eta(\xi,\eta)}\frac{\partial u}{\partial\eta} = 0 \qquad at \qquad \eta = \frac{\pi}{2} \tag{26}$$

$$\frac{1}{h_\xi(\xi,\eta)}\frac{\partial u}{\partial\xi} = 0 \qquad at \qquad \xi = 0 \tag{27}$$

$$u = \beta_s = -\frac{\beta_v Kn}{c\sqrt{cosh^2\xi - cos^2\eta}}\frac{\partial u}{\partial\xi} \qquad at \qquad \xi = \xi_0 \tag{28}$$

3.3. Analytical solution

As seen from the above system of equations, the boundary condition Eq. (28) is non-homogeneous. Therefore, filtering is applied to eliminate non-homogeneity. We define a one-dimentional problem in the ξ-direction such that it satisfies the boundary conditions Eqs. (25)-(28). Therefore, the velocity at the left and right walls vanishes for the original problem.

$$u(\xi,\eta) = \tilde{u}(\xi,\eta) + u_\xi(\xi) \tag{29}$$

where u_ξ, filtering function, satisfies the following systems:

$$\frac{d^2 u_\xi}{d\xi^2} = 0 \tag{30}$$

$$\frac{du_\xi}{d\xi} = 0 \qquad at \qquad \xi = 0 \tag{31}$$

$$u_\xi = \beta_s \qquad at \qquad \xi = \xi_0 \tag{32}$$

The solution of the above equation can easily be written as

$$u_\xi = \beta_s \tag{33}$$

The governing equation and boundary conditions take the following forms after the substitution of Eq. (29) into Eqs. (25)-(28)

$$\frac{\partial^2\tilde{u}}{\partial\xi^2} + \frac{\partial^2\tilde{u}}{\partial\eta^2} = c^2\left(cosh^2\xi - cos^2\eta\right)P \tag{34}$$

$$\frac{\partial\tilde{u}}{\partial\eta} = 0 \qquad at \qquad \eta = 0 \tag{35}$$

$$\frac{\partial \tilde{u}}{\partial \eta} = 0 \qquad at \qquad \eta = \frac{\pi}{2} \tag{36}$$

$$\frac{\partial \tilde{u}}{\partial \xi} = 0 \qquad at \qquad \xi = 0 \tag{37}$$

$$\tilde{u} = 0 \qquad at \qquad \xi = \xi_0 \tag{38}$$

It can be noted that when the filtering scheme is applied, the boundary conditions are written properly to carry out the changes along the computation. As we have four homogeneous boundary conditions, the Eigenvalue problem can be defined along ξ-direction and the other two conditions can be implemented at the end. The appropriate eigenvalue problem related to the velocity problem is given:

$$\frac{d^2\psi(\xi)}{d\xi^2} + \mu^2 \psi(\xi) = 0 \tag{39}$$

with the boundary conditions:

$$\frac{d\psi(\xi)}{d\xi} = 0 \qquad at \qquad \xi = 0 \tag{40}$$

$$\psi(\xi) = 0 \qquad at \qquad \xi = \xi_0 \tag{41}$$

The eigenvalues and eigenfunctions associated to this problem are:

$$\mu_n = \frac{(2n-1)\pi}{2\xi_0} \qquad (n = 1, 2, 3, \ldots) \tag{42}$$

$$\psi_n(\xi) = \cos\left(\mu_n \xi\right) \tag{43}$$

where normalization integrals given by:

$$N_n = \int_0^{\xi_0} \psi_n^2(\xi)\, d\xi = \frac{\xi_0}{2} \tag{44}$$

The transform and inversion formulas are written as

Transform:

$$\bar{\tilde{u}}\left(\mu_n, \eta\right) = \int_0^{\xi_0} \frac{\psi_n\left(\mu_n, \xi\right)}{N_n^{1/2}} \tilde{u}\left(\xi, \eta\right) d\xi \tag{45}$$

Inversion:

$$\tilde{u}\left(\xi, \eta\right) = \sum_{n=1}^{\infty} \frac{\psi_n\left(\mu_n, \xi\right)}{N_n^{1/2}} \bar{\tilde{u}}\left(\mu_n, \eta\right) \tag{46}$$

The transformation process starts by applying $\int_0^{\xi_0} \psi_n d\xi$ to every term in Eq. (34)

$$\int_0^{\xi_0} \frac{\partial^2 \tilde{u}}{\partial \xi^2} \psi_n d\xi + \int_0^{\xi_0} \frac{\partial^2 \tilde{u}}{\partial \eta^2} \psi_n d\xi = \int_0^{\xi_0} c^2 \left(cosh^2 \xi - cos^2 \eta\right) P \psi_n d\xi \tag{47}$$

The inversion and transform formulas and the Eigen value problem are obtained using integration by parts technique are utilized to evaluate the integrals in Eq. (47). Therefore, Eq. (47) is obtained in the following transformed form

$$\frac{d^2 \bar{\tilde{u}}}{d\eta^2} - \mu_n^2 \bar{\tilde{u}} = c^2 \left\{ \frac{(-1)^{n-1} \mu_n cosh\left(2\xi_0\right)}{2N_n^{1/2}\left(4 + \mu_n^2\right)} - \frac{(-1)^{n-1} cos\left(2\eta\right)}{2N_n^{1/2}\mu_n} \right\} P \tag{48}$$

Transformation of the boundary conditions yields Eq. (45)

$$\frac{d\bar{\tilde{u}}}{d\eta} = 0 \qquad at \qquad \eta = 0 \tag{49}$$

$$\frac{d\bar{\tilde{u}}}{d\eta} = 0 \qquad at \qquad \eta = \frac{\pi}{2} \tag{50}$$

The solution to the non-homogeneous ordinary differential equation, Eq. (48) is obtained analytically and after some rearrangements, the following appropriate forms are obtained.

$$\bar{\tilde{u}}\left(\mu_n, \eta\right) = c^2 A_n \left(cos\left(2\eta\right) - cosh\left(2\xi_0\right)\right) P \tag{51}$$

where

$$A_n = \frac{(-1)^{n-1}}{2N_n^{1/2}\mu_n\left(4+\mu_n^2\right)} \tag{52}$$

Then, the inversion formula is applied to obtain $\tilde{u}$

$$\tilde{u}\left(\xi,\eta\right) = \sum_{n=1}^{\infty} \frac{\left[c^2 A_n\left(cos\left(2\eta\right) - cosh\left(2\xi_0\right)\right)P\right] cos\left(\mu_n\xi\right)}{N_n^{1/2}} \tag{53}$$

The final form of the velocity profile is obtained by summing Eqs. (29) and (53)

$$u\left(\xi,\eta\right) = \sum_{n=1}^{\infty} \frac{\left[c^2 A_n\left(cos\left(2\eta\right) - cosh\left(2\xi_0\right)\right)P\right] cos\left(\mu_n\xi\right)}{N_n^{1/2}} + \beta_s \tag{54}$$

The value of P is still unknown in Eq. (54), which is obtained by implementing the definition of mean velocity

$$u_m^* = \frac{1}{\pi a^* b^*} \iint_{\Gamma^*} u^*\left(x^*, y^*\right) dx^* dy^* \tag{55}$$

Once Eq. (54) is substituted into Eq. (55), P is evaluated as follows:

$$P = \frac{1-\beta_s}{c^2\left(I_1+I_2\right)} \tag{56}$$

where

$$I_1 = \frac{-2cosh^2\left(2\xi_0\right)}{\varepsilon cosh^2\xi_0} \sum_{n=1}^{\infty} \mu_n^2 A_n^2 \tag{57}$$

$$I_2 = \frac{-1}{\varepsilon cosh^2\xi_0} \sum_{n=1}^{\infty} \left(4+\mu_n^2\right) A_n^2 \tag{58}$$

The only unknown left is the slip coefficient. To achieve β_s as a function of the slip parameter $\beta = \beta_v Kn$, using Eq. (28) the following expression for slip coefficient in non-dimensional form is obtained. Here that the average value of β_s is calculated by integrating over the length

$$\beta_s = \frac{1}{2\pi} \int_0^{2\pi} \frac{2\beta_v Kn I_3\left(cosh^2\xi_0 - cos^2\eta\right)}{c\sqrt{cosh^2\xi_0 - cos^2\eta} + 2\beta_v Kn I_3\left(cosh^2\xi_0 - cos^2\eta\right)} d\eta \tag{59}$$

where

$$I_3 = \frac{1}{\left(I_1+I_2\right)} \sum_{n=1}^{\infty} (-1)^n \frac{\mu_n A_n}{N_n^{1/2}} \tag{60}$$

In order to overcome the difficulty by term

$$h_\xi\left(\xi_0,\eta\right) = c\sqrt{cosh^2\xi_0 - cos^2\eta} \tag{61}$$

We use the following binomial series to approximate Eq. (61)

$$(1+x)^a = 1 + \sum_{n=1}^{\infty} \frac{a(a-1)(a-2)...(a-n+1)}{n!} x^n \qquad -1 < x < 1 \tag{62}$$

The Eq. (61) can be written as:

$$h_\xi\left(\xi_0,\eta\right) = c(cosh^2\xi_0 - cos^2\eta)^{1/2} = ccosh\xi_0\left(1 - \frac{cos^2\eta}{cosh^2\xi_0}\right)^{1/2} \tag{63}$$

assuming the first N terms appropriate of expansion Eq. (63), we get

$$\begin{aligned}\beta_s = \tfrac{1}{2\pi}\textstyle\int_0^{2\pi} \{\left[2\beta_v Kn I_3\left(cosh^2\xi_0 - cos^2\eta\right)\right] \Big/ [ccosh\xi_0 \\ \times\left(1 + \textstyle\sum_{n=1}^{N} \frac{(1)(-1)(-3)...(1-2(n+1))}{2^n n!}\left(-\frac{cos^2\eta}{cosh^2\xi_0}\right)^n\right) + 2\beta_v Kn I_3\left(cosh^2\xi_0 - cos^2\eta\right)]\} d\eta\end{aligned} \tag{64}$$

Because finding analytical solution of Eq. (64) is difficult, we use 6 to 12 points formulas of Gauss-Legendre and Gauss-Lobatto numerical integration for $N > 3$. In most cases, we choice 6-points formula of Gauss-Lobatto and $N = 3$ (Davis and Rabinowitz [29] and Jain and Chawlas [30]) to approximate Eq. (64).

4. Slip flow models

By obtaining the velocity distribution $u\left(\xi,\eta\right)$ and mean velocity u_m , the friction factor and Reynolds number product may be defined using the simple expression of the Poiseuille number Churchill [34], Muzychka and

Yovanovich [35, 36] and Duan and Yovanovich [22]

$$Po_{L_c} = \frac{\tau_m L_c}{\mu u_m} = \frac{\left(-\frac{A_c}{P_c}\frac{dp}{dz}\right)L_c}{\mu u_m} = \frac{fRe_{L_c}}{2} \tag{65}$$

The above grouping Po is interpreted as the dimensionless average wall shear stress.

4.1. Characteristic length scale

It is clear that all definitions grouping Po (Eq. (65)) depend on the choice of the characteristic length scale (L_c). The most frequently recommended length scale is the hydraulic diameter defined as:

$$L_c = D_h = \frac{4A_c}{P_c} \tag{66}$$

Where A_c and P_c are calculated in the present paper as:

$$A_c = \pi ab \tag{67}$$

$$P_c = 4aE(e) \tag{68}$$

However, its use in laminar flow has been questioned by White [37]. In an earlier work Yovanovich and Muzychka [38], the authors addressed this issue using dimensional analysis. It was determined that the widely used concept of the hydraulic diameter was inappropriate for laminar flow, and the authors proposed using $L_c = \sqrt{A_c}$ as a characteristic length scale by considering other problems in mathematical physics for which the Poisson equation applies (e.g., Eq. (1)). A more detailed discussion and analysis on the use of $L_c = \sqrt{A_c}$ may be found in Muzychka [39] and in Bahrami et al. [40]. Rrecently, Duan and Muzychka [20, 21] and Muzychka and Edge [41] have shown that the square root of flow area is also more appropriate for non-dimensionalizing gaseous slip flows and non-Newtonian flows, respectively.

4.2. Elliptic friction factor and Reynolds number product

We define the friction factor Reynolds number as a product of which results after employing different characteristic lengths for elliptic microchannels for slip flow. The fRe_{D_h} is given by the following relationship:

$$fRe_{D_h} = \frac{2\left(-\frac{A_c}{P_c}\frac{dp}{dz}\right)D_h}{\mu u_m} \tag{69}$$

After substitution for the mean velocity, the following relationship is obtained:

$$fRe_{D_h} = -\frac{\pi^2\varepsilon^2}{2E^2(e)}\frac{1-\beta_s}{\left(1-\varepsilon^2\right)(I_1+I_2)} \tag{70}$$

Similarly, the following relationship is obtained for $fRe_{\sqrt{A_c}}$

$$fRe_{\sqrt{A_c}} = -\frac{\pi^{3/2}\varepsilon^{3/2}}{2E(e)}\frac{1-\beta_s}{\left(1-\varepsilon^2\right)(I_1+I_2)} \tag{71}$$

It can be demonstrated that the limit of Eqs. (70) and (71) for $\varepsilon = b/a \to 1$ corresponds to circular microchcnnels Kennard [42] where $E(e)$ is the complete elliptical integral of the second kind Abramowitz [43]. It can also be shown that Eqs. (70) and (71), reduces to theirs continuum flow limits as $\beta \to 0$

$$\left(fRe_{D_h}\right)_{ns} = \frac{\pi^2\varepsilon^2}{2E^2(e)}\frac{-1}{\left(1-\varepsilon^2\right)(I_1+I_2)} \tag{72}$$

$$\left(fRe_{\sqrt{A_c}}\right)_{ns} = \frac{\pi^{3/2}\varepsilon^{3/2}}{2E(e)}\frac{-1}{\left(1-\varepsilon^2\right)(I_1+I_2)} \tag{73}$$

Shah and London [44] have shown that for $\varepsilon = b/a \to 1$

$$\begin{cases} fRe_{D_h} \to 16 \\ fRe_{\sqrt{A_c}} \to 14.18 \end{cases} \tag{74}$$

5. Results and discussion

The values of slip coefficient, non-dimensional slip velocity with different aspect ratio ε and slip parameter β are shown in Table 1 for $0 \le \beta \le 0.12$ and $0.1 \le \varepsilon \le 1$. One can observe that the values of β_s increase with an increase of β for the same aspect ratio ε as shown in Table 1. The variation of slip coefficient for elliptic micro-channels reported

Table 1. The values of slip coefficient for varying ε and β

ε	0.100	0.300	0.500	0.700	0.900	1.000
β				β_s		
0.000	0.000	0.000	0.000	0.000	0.000	0.000
0.001	0.011	0.010	0.009	0.008	0.008	0.008
0.020	0.188	0.171	0.154	0.143	0.138	0.138
0.040	0.316	0.291	0.266	0.250	0.243	0.242
0.060	0.409	0.380	0.351	0.333	0.325	0.324
0.080	0.480	0.449	0.418	0.399	0.391	0.390
0.100	0.535	0.503	0.472	0.453	0.445	0.444
0.120	0.580	0.548	0.517	0.499	0.491	0.490

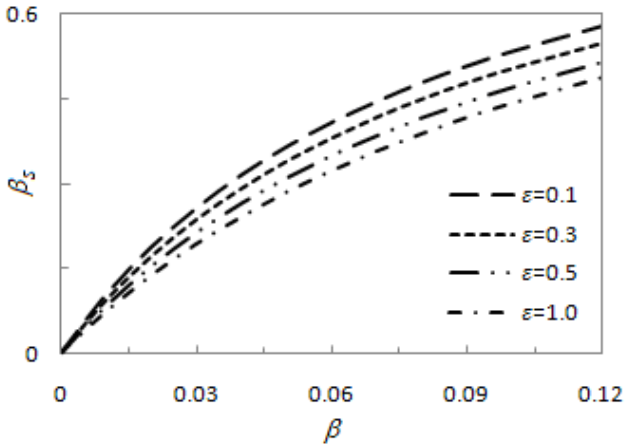

Fig. 2. The variation of slip coefficient with slip parameter

Table 2. Comparison of fully developed fRe_{D_h} for elliptic microchannels

β	0.000		0.001		0.010		0.050		0.100	
ε	Duan [21]	Present	Duan [21]	Present	Duan [21]	Present	Duan [21]	Present	Duan [21]	Present
0.100	19.314	19.314	19.093	19.093	17.314	17.314	12.250	12.250	8.979	8.979
0.200	18.602	18.602	18.399	18.399	16.758	16.758	12.023	12.023	8.913	8.913
0.300	17.896	17.896	17.712	17.712	16.219	16.219	11.834	11.834	8.886	8.886
0.400	17.294	17.294	17.128	17.128	15.767	15.767	11.693	11.693	8.881	8.881
0.500	16.823	16.823	16.671	16.671	15.418	15.418	11.591	11.591	8.880	8.880
0.600	16.479	16.479	16.337	16.337	15.164	15.164	11.517	11.517	8.879	8.879
0.700	16.244	16.244	16.109	16.109	14.991	14.991	11.470	11.470	8.879	8.879
0.800	16.098	16.098	15.968	15.968	14.884	14.884	11.442	11.442	8.880	8.880
0.900	16.022	16.022	15.894	15.894	14.830	14.830	11.430	11.430	8.885	8.885
1.000	16.000	16.000	15.873	15.873	14.815	14.815	11.429	11.429	8.889	8.889

as β_s are plotted versus the slip parameter (β) and is shown in Fig. 2. For the same slip parameter β, as the aspect ratio becomes smaller the value of slip coefficient increases.

The results of friction factor and Reynolds number product for hydraulic diameter fRe_{D_h} with different aspect ratio ε and slip parameter β are shown in Table 2. One can observe that the values of the fRe_{D_h} as shown in Table 2, decrease with an increase of β for the same aspect ratio ε. Ebert and Sparrow [11] and Sreekanth [45] theoretically proved that the gas rarefaction leads to a reduction of the Po for increasing β. The fRe_{D_h} values decrease with an increase of ε for the same β for most of the cases.

Similarly, the data for elliptic micro-channels as $fRe_{\sqrt{A_c}}$ reported are same as for fRe_{D_h} as shown in Table 3.

Table 3. Comparison of fully developed $fRe_{\sqrt{A_c}}$ for elliptic microchannels

β	0.000		0.001		0.010		0.050		0.100	
ε	Duan [21]	Present	Duan [21]	Present	Duan [21]	Present	Duan [21]	Present	Duan [21]	Present
0.100	35.009	35.009	34.609	34.609	31.384	31.384	22.205	22.205	16.277	16.277
0.200	24.653	24.653	24.384	24.384	22.209	22.209	15.934	15.934	11.812	11.812
0.300	20.213	20.213	20.006	20.006	18.319	18.319	13.366	13.366	10.037	10.037
0.400	17.752	17.752	17.581	17.581	16.185	16.185	12.002	12.002	9.116	9.116
0.500	16.256	16.256	16.109	16.109	14.898	14.898	11.200	11.200	8.581	8.581
0.600	15.320	15.320	15.188	15.188	14.097	14.097	10.308	10.708	8.255	8.255
0.700	14.739	14.739	14.617	14.617	13.603	13.603	10.407	10.407	8.056	8.056
0.800	14.400	14.400	14.284	14.284	13.314	13.314	10.235	10.235	7.944	7.944
0.900	14.229	14.229	14.116	14.116	13.170	13.170	10.151	10.151	7.891	7.891
1.000	14.180	14.180	14.067	14.067	13.129	13.129	10.129	10.129	7.878	7.878

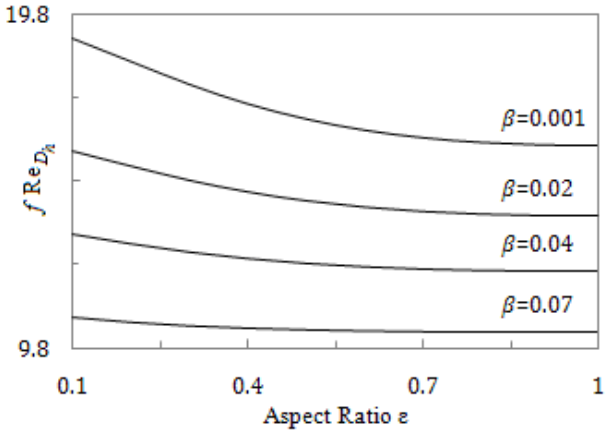

Fig. 3. Fully developed fRe_{D_h} for elliptic microchannels with aspect ratio for $0.001 \le \beta \le 0.07$

When $\varepsilon = b/a \to 1$, the friction factor and Reynolds number product results reduce to circular microchannels. Table 2 and Table 3, show that the present values of friction factor and Reynolds number product (fRe) for elliptic micro-channels are in good agreement and also improvement with the previous results Duan and Muzychka [20, 21] for elliptic micro-channels where the maximum difference is smaller than 0.2%. The value for elliptic microchannels reported as fRe_{D_h} are plotted versus the aspect ratio (ε) is shown in Figs. 3 and 4. The data decrease with increasing values of ε for $0.001 \le \beta \le 0.07$ and $0.08 \le \beta \le 0.12$ as shown in Figs. 3 and 4.

In the next step, all data is converted from fRe_{D_h} to $fRe_{\sqrt{A}}$ and re-plotted with respect to aspect ratio (ε). When this is done as shown in Figs. 5 and 6, the data follow closely a similar trend where the values decrease with increasing values of ε while $0.001 \le \beta \le 0.07$ and $0.08 \le \beta \le 0.12$ in as shows in Figs. 5 and 6.

The comparison of Fig. 3 and Fig. 5, Fig. 4 and Fig. 6 demonstrate that the square root of elliptic cross-sectional area is a more appropriate characteristic length scale than the hydraulic diameter for non-dimensionalizing the fully developed laminar flow data which β greater than 0.001.

Table 4 presents the values of the normalized Poiseuille number for elliptic microchannels for some values of the slip parameter between 0.001 and 0.1 for which gas rarefaction reduces the friction between the gas and the microchannel walls. The reduction of the normalized Poiseuille number is stronger for elliptic microchannels with small channel aspect ratios. Further, Table 4 show that the present values of normalized Poiseuille number (Po) for elliptic microchannels, which are in good agreement with the previous results (Duan and Muzychka [20, 21]) of elliptic microchannels, which the maximum difference is smaller than 0.2% and (Morini et al. [15]) of rectangular microchannels, which the maximum difference is smaller than 1.7% in most cases for $0 \le \beta \le 0.12$.

The effects of slip are illustrated by plotting the normalized Poiseuille number (Po/Po_{ns}) as a function of the slip parameter and aspect ratio, where Po_{ns} represents the no-slip flow. Fig. 7 shows the normalized Poiseuille number results for elliptic microchannels as a function of aspect ratio ε and β. From an inspection of the graphs, it is seen that Po/Po_{ns} decreases as the rarefaction becomes greater. The Poiseuille number reduction depends on the geometry of

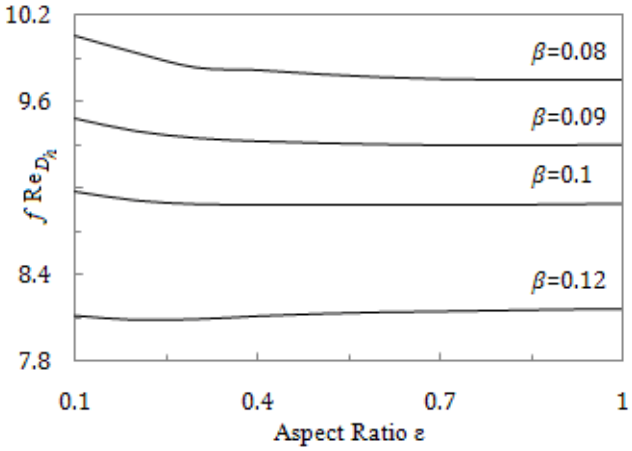

Fig. 4. Fully developed fRe_{D_h} for elliptic microchannels with aspect ratio for $0.08 \le \beta \le 0.12$

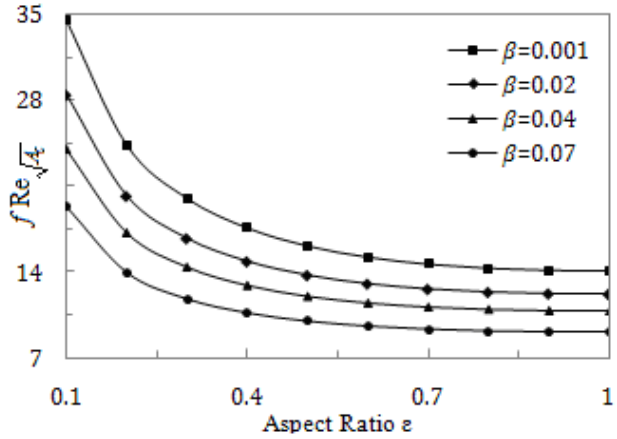

Fig. 5. Fully developed $fRe_{\sqrt{A_c}}$ for elliptic microchannels with aspect ratio for $0.001 \le \beta \le 0.07$

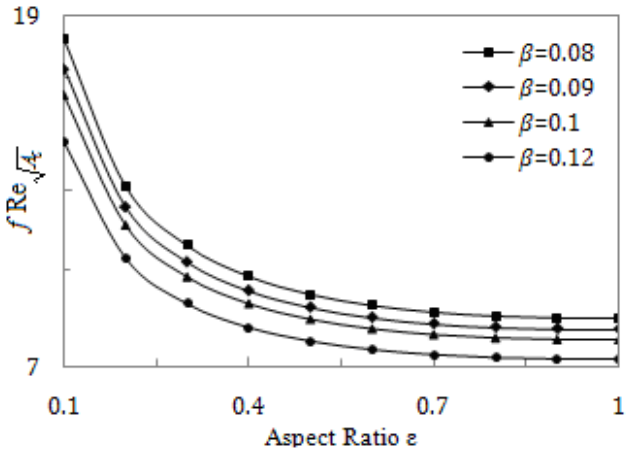

Fig. 6. Fully developed $fRe_{\sqrt{A_c}}$ for elliptic microchannels with aspect ratio for $0.08 \le \beta \le 0.12$

cross-section and on the slip parameter.

Table 4. Comparison of normalized Poiseulle numbers for rectangular/elliptic microchannels

β	0.001			0.010			0.050			0.100		
ε	Morini [15]	Duan [21]	Present	Morini [15]	Duan [21]	Present	Morini [15]	Duan [21]	Present	Morini [15]	Duan [21]	Present
0.1	0.939	0.939	0.939	0.901	0.896	0.896	0.645	0.634	0.634	0.477	0.465	0.465
0.2	0.990	0.939	0.939	0.907	0.901	0.901	0.662	0.646	0.646	0.496	0.479	0.479
0.3	0.990	0.990	0.990	0.912	0.906	0.906	0.677	0.661	0.661	0.514	0.497	0.497
0.4	0.991	0.990	0.990	0.917	0.912	0.912	0.690	0.676	0.676	0.529	0.514	0.514
0.5	0.991	0.991	0.991	0.920	0.916	0.916	0.700	0.689	0.689	0.541	0.523	0.523
0.6	0.992	0.991	0.991	0.923	0.920	0.920	0.707	0.699	0.699	0.551	0.539	0.539
0.7	0.992	0.992	0.992	0.924	0.923	0.923	0.713	0.706	0.706	0.557	0.547	0.547
0.3	0.992	0.992	0.992	0.925	0.925	0.925	0.716	0.711	0.711	0.562	0.552	0.552
0.9	0.992	0.992	0.992	0.925	0.926	0.926	0.716	0.713	0.713	0.564	0.555	0.555
1.0	0.992	0.992	0.992	0.926	0.926	0.926	0.719	0.714	0.714	0.565	0.556	0.556

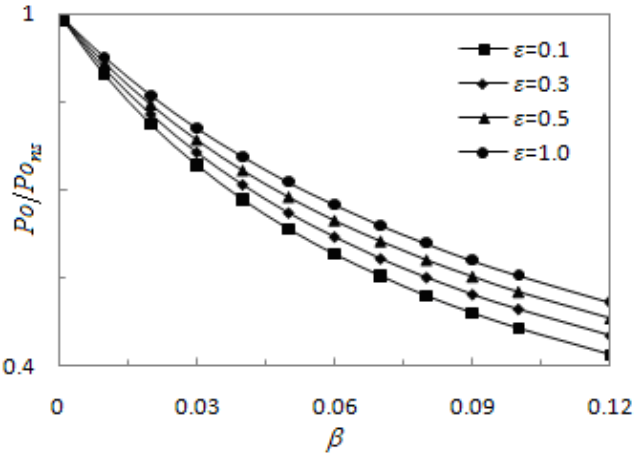

Fig. 7. Normalized *placePo* results as a function of ε and β for elliptic microchannels

6. Conclusion

This paper investigates fully developed gaseous slip flow with the first-order velocity slip boundary conditions at the channel walls using elliptic cylindrical coordinate system on applying the integral transform technique. It was shown that the present values of friction factor and Reynolds number product (fRe) and normalized Poiseuille number (Po) for elliptic micro-channels are in good agreement for smaller aspect ratios with the previous results for elliptic and rectangular microchannels. The maximum difference of the predicted results was found to be within 0.2% and 1.7% for elliptic and rectangular microchannels, respectively. As the prediction of the model very close to the exact value, this model can be used to calculate mass flow rate and pressure distribution of slip flow in elliptic microchannels.

Acknowledgements

The authors gratefully acknowledge the financial support of this work by the Kermanshah branch, Islamic Azad University of Iran and its Digital Library.

References

[1] G.E. Karniadakis, A. Beskok, N. Aluru, Microflows and Nanoflows: Fundamentals and Simulation, Springer, New York, 2005.

[2] M. Gad-el-Hak, The Fluid Mechanics of Microdevices-the Freeman Scholar Lecture, ASME J. Fluids Eng. 121 (1)(1999) 5-33.
[3] J. Jang, S.T. Werely, Effective Heights and Tangential Momentum Accommodations Coefficients of Gaseous Slip Flows in Deep Reactive Ion Etching Rectangular Microchannels, J. Micromech Microeng. 16 (3)(2006) 493-504.
[4] E.B. Arkilic, M.A. Schmidt, K.S. Breuer, Gaseous Slip Flow in Long Microchannels. J. Microelectromech System. 6 (2)(1997) 167–178.
[5] J. Liu, Y.C. Tai, C.M. Ho, MEMS for Pressure Distribution Studies of Gaseous Flows in Microchannels, Proceedings of IEEE International Conference on Micro Electro Mech. Systems, Amsterdam, Netherlands, (1995) 209–215.
[6] J. Pfahler, J. Harley, H. Bau, J.N. Zemel, Gas and Liquid Transport in Small Channels, Proceedings of ASME Microstructures, Sensors and Actuators, and Systems, 19 (1990) 149-157.
[7] J. Pfahler, J. Harley, H. Bau, J.N. Zemel, Gas and Liquid Flow in Small Channels, Proceedings of ASME Micromechanical Sensors, Actuators, and Systems, 32 (1991) 49-59.
[8] J. Harley, Y. Huang, H. Bau, J.N. Zemel, Gas Flows in Microchannels, J. Fluid Mechanics. 284 (1995) 257-274.
[9] S. Wu, J. Mai, Y. Zohar, Y.C. Tai, C.M. Ho, A Suspended Microchannel With Integrated Temperature Sensors for High Pressure Studies, Proceedings of IEEE Workshop on MicroElectro Mechanical Systems, Heidelberg, Germany, (1998) 87-92.
[10] T. Araki, M.S. Kim, I. Hiroshi, K. Suzuki, An Experimental Investigation of Gaseous Flow Characteristics in Microchannels, Proceedings of International Conference on Heat Transfer and Transport Phenomena in Microscale. Begell House, New York, (2000) 155-161.
[11] W.A. Ebert, E.M. Sparrow, Slip Flow in Rectangular and Annular Ducts, ASME J. Basic Eng. 87 (4)(1965) 1018-1024.
[12] E.G.R. Eckert, R.M. Drake, Analysis of Heat and Mass Transfer, McGraw-Hill, New York, 1972.
[13] A.A. Rostami, placeN. Saniei, A.S. Majumder, Liquid Flow and Heat Transfer in Microchannels: A Review, Int. J. Heat Technol. 18 (2)(2000) 59-68.
[14] A.A. Rostami, A.S. Majumder, N. Saniei, Flow and Heat Transfer for Gas Flowing in Microchannels: A Review, Heat Mass Transf. 38 (4-5) (2002) 359-367.
[15] G.L. Morini, M. Spiga, P. Tartarini, The Rarefaction Effect on the Friction Factor of Gas Flow in Micro/Nano-Channels, Superlattices Microstruct. 35 (3-6) (2004) 587-599.
[16] C. Aubert, S. Colin, Higher order Boundary for gaseous flows in rectangular microduct, Microscale Thermophysical Engrg. (2001) 41-54.
[17] R.G. Deisler, An analysis of second-order slip flow and temperature jump conditions for rarefied gases, Int. J. Heat Mass Transfer. 7 (1964) 681-694.
[18] S. Colin, P. Lalonde, R. Caen, Validation of a Second-Order Slip Flow Model in rectangular Microchannels, Heat Transf. Eng. 25 (3)(2004) 23-30.
[19] R.F. Barron, X. Wang, T.A. Ameel, R.O. Warrington, The Graetz Problem Extended to Slip-Flow, Int. J. Heat Mass Transf. 40 (8)(1997) 1817-1823.
[20] Z. Duan, Y.S. Muzychka, Slip Flow in Non-Circular Microchannels, Microfluidics Nanofluidics. 3 (4)(2007) 473-484.
[21] Z. Duan, Y.S. Muzychka, Slip Flow in Elliptic Microchannels, Int. J, Therm. Sci. 46 (11)(2007) 1104-1111.
[22] Z. Duan, M.M. Yovanovich, Models for Gaseous Slip Flow in Circular and Noncircular Microchannels, Proceedings of ASME 2010 3rd Joint US-European Fluids Engineering Summer Meeting and 8th International Conference on Nanochannels, Microchannels and Minichannels, August 1-5, 2010, Montreal, Canada, paper No. FEDSM-ICNMM2010-30320 (2010) 421-431.
[23] G. Tunc, Y. Bayazitoglu, Heat transfer in rectangular microchannels, Int. J. Heat and Mass Transfer. 45 (2002) 765-773.
[24] F. Tahmouresi, S.K. Das, Analytical Modeling of Gaseous Slip Flow in Parabolic Microchannels, ASME J. Fluids Eng. 136 (7)(2014) 071201.
[25] K.V. Reddy, M.G. Reddy, Velocity slip and joule heating effects on MHD peristaltic flow in a porous medium, International Journal of Advances in Applied Mathematics and Mechanics 2(2) (2014) 126 âĂŞ 138.
[26] S.P. Anjali Devi, D.V. Kumari, Numerical investigation of slip flow effects on unsteady hydromagnetic flow over a stretching surface with thermal radiation, International Journal of Advances in Applied Mathematics and Mechanics 1(4) (2014) 20 âĂŞ 32.
[27] P. Ghasemi Moakher, M. Abbasi , M. Khaki, New analytical solution of MHD fluid flow of fourth grade fluid through the channel with slip condition via collocation method, International Journal of Advances in Applied Mathematics and Mechanics 2(3) (2015) 87 âĂŞ 94.
[28] G.B. Arfken, Mathematical Methods for Physicists, Acad. Press, USA, 1970.
[29] J.C. Maxwell, On Stresses in Rarefied Gases Arising From Inequalities of Temperature Philos, Trans. Royal Soc. 170 (1879) 231–256.
[30] W.M. Rohsenow, H. Y. Choi, Heat, Mass and Momentum Transfer, Prentice Hall, New York, 1961.
[31] J.C. Shih, C. Ho, J. Liu, Y. Tai, Monatomic and Polyatomic gas flow through uniform microchannels, in: National Heat Transfer Conference, Micro Electro Mechanical Systems (MEMS), Atlanta, GA, DSC. 59 (1996) 197-203.
[32] P. Davis, P. Rabinowitz, Numerical Integration, Blaisdell, New York, 1967.
[33] M.K. Jain, M.M. Chawlas, Numerical Analysis for Scientists and Engineers, S.B.W Publishers, New Delhi, 1971.

[34] S.W. Churchill, Viscous Flows: The Practical Use of Theory, Butterworth- Heinemann, Boston, 1988.
[35] Y.S. Muzychka, M.M. Yovanovich, Laminar Flow Friction and Heat Transfer in Non-Circular Ducts and Channels Part I: Hydrodynamic Problem, Compact Heat Exchangers, Proceedings of the International Symposium on Compact Heat Exchangers, Grenoble, France, August 24. (2002) 123–130.
[36] Y. S. Muzychka, M. M. Yovanovich, Laminar Flow Friction and Heat Transfer in Non-Circular Ducts and Channels Part II: Hydrodynamic Problem, Compact Heat Exchangers, Proceedings of the International Symposium on Compact Heat Exchangers, Grenoble, France, August 24. (2002) 131-139.
[37] F.M. White, Viscous Fluid Flow, McGraw-Hill, New York, 1974.
[38] M.M. Yovanovich, Y.S. Muzychka, Solutions of Poisson equation with in singly and doubly prismatic connected domains, National Heat Transfer Conference, AIAA (1970) Paper No. 97-3880.
[39] Y.S. Muzychka, Analytical and Experimental Study of Fluid Friction and Heat Transfer in Low Reynolds Number Flow Heat Exchangers, Ph.D. thesis, University of Waterloo, Waterloo, ON, Canada, 1999.
[40] M. Bahrami, M.M. Yovanovich, J.R. Culham, Pressure Drop of Fully Developed, Laminar Flow in Microchannel of Arbitrary Cross-Section, ASME J. Fluids Eng. 128 (5)(2006) 1036-1044.
[41] Y.S. Muzychka, J. Edge, Laminar Non-Newtonian Fluid Flow in Non- Circular Ducts and Microchannels, ASME J. Fluids Eng., 130 (11)(2008) 111201.
[42] E.H. Kennard, Kinetic Theory of Gases, McGraw–Hill, New York, 1938.
[43] M. Abramowitz, I.A. Stegun, Handbook of Mathematical Functions, Courier Dover Publications, 1965.
[44] R.K. Shah, A.L. London, Laminar Flow Forced Convection in Ducts, Academic Press, New York, 1978.
[45] A.K. Sreekanth, Slip flow through long circular tubes, Proceedings of the Sixth International Symposium on Rarefied Gas Dynamics, Academic Press, San Diego, CA. (1969) 667-680.